Citation
Cui, L. and Dale, B. and Allison, G. and Li, M. 2021. Design and Development of An Instrumented Knee Joint for Quantifying Ligament Displacements. Journal of Medical Devices, Transactions of the ASME. 15 (3): ARTN 031009. http://doi.org/10.1115/1.4051440

Design and Development of An Instrumented Knee Joint for Quantifying Ligament Displacements

Lei Cui
Schoo of Civil & Mechanical Engineering
Curtin University
Perth, Western Australia
Email: lei.cui@curtin.edu.au

Brody Dale
Schoo of Civil & Mechanical Engineering
Curtin University
Perth, Western Australia
Email: brodytdale@gmail.com

Garry Allison
Curtin Graduate Research School
Curtin University
Perth, Western Australia
Email: G.Allison@curtin.edu.au

Min Li
School of Mechanical Engineering
Xi'an Jiaotong University
Xi'an, China
Email: min.li@xjtu.edu.cn

ABSTRACT

Recently robotic assistive leg exoskeletons have gained popularity because an increased number of people crave for powered devices to run faster and longer or carry heavier loads. However, these powered devices have the potential to impair knee ligaments. This work was aimed to develop an instrumented knee joint via rapid prototyping that measures the displacements of the four major knee ligaments—the anterior cruciate

ligament (ACL), posterior crucial ligament (PCL), medial collateral ligament (MCL), and lateral collateral ligament (LCL)—to quantify the strain experienced by these ligaments. The knee model consists of a femur, lateral and medial menisci, and a tibia-fibula, which were printed from 3D imaging scans. Non-stretchable cords served as main fiber bundles of the ligaments with their desired stiffnesses provided by springs. The displacement of each cord was obtained via a rotary encoder mechanism, and the leg flexion angle was acquired via a closed-loop four-bar linkage of a diamond shape. The displacements were corroborated by published data, demonstrating the profiles of the displacement curves agreed with known results. The paper shows the feasibility of developing a subject-specific knee joint via rapid prototyping that is capable of quantifying the ligament strain via rapid prototyping.

NOMENCLATURE

ACL Anterior Cruciate Ligament.

PCL Posterior Cruciate Ligament.

MCL Medial Collateral Ligament.

LCL Lateral Collateral Ligament.

1 INTRODUCTION

The human musculoskeletal system is comprised of bones of the skeleton, muscles, cartilage, tendons, ligaments, and other connective tissues, providing form, stability, support, and movement of the body. The bones are connected through joints, inside which cartilage connects one bone to another as in the spine, or provides load-bearing as in the knee joint.

The knee is the largest and most complex joint in the body. The knee joint connects the femur (the thigh bone) to the tibia (the shin bone), on the lateral side of which runs the fibula (the smaller bone in the lower leg). The patella (the knee cap) is the third bone of the knee, protecting its front. The knee allows the movements between the lower leg relative to the thigh while supporting the body's weight [1].

The four main ligaments in the knee joint connect the femur and the tibia-fibula. In the centre

of the knee, the anterior cruciate ligament (ACL) controls rotation and forward movement of the tibia; the posterior crucial ligament (PCL) controls backward movement of the tibia. The medial collateral ligament (MCL) and lateral collateral ligament (LCL) provide stability to the inner and outer knee, respectively, as in Fig. 1.

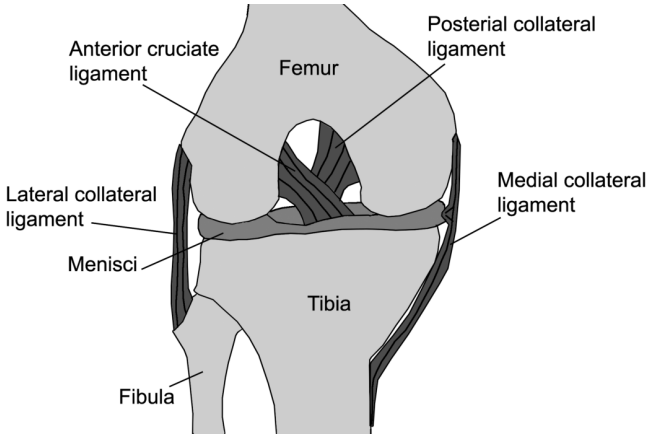

Fig. 1. The ligaments in the knee joint

The four main ligaments stabilize the knee, which is crucial in many daily activities, such as walking, sitting, and standing. Hence, investigating the strain behaviours of the ligaments is essential to the prevention of knee injuries.

Extensive research has gone into characterizing the properties of the knee ligaments and their roles in knee dynamics. Cadaveric tests have been used to identify the mechanical properties of the ligaments. Destructive tensile testing machines have been used to measure and compare the structural properties of the ligaments of the knees harvested from human cadaveric knees. After preconditioning, the specimens were extended to failure in tensile testing machines [2, 3].

It is common to measure ligament displacement, which is then used to calculate the ligament strain. For example, a differential variable reluctance transducer (DVRT), which is an inductive displacement sensor, was sewn to the side of the ACL to measure its displacement, which subsequently was used to infer the strain in a gait cycle while the muscle forces were simulated using pretensioned steel cables [4].

Other displacement sensors are also used for this purpose. For instance, a Hall-Effect trans-

ducer, which senses displacement using magnetic field, was attached to the MCL of human autopsy to measure the displacement of the MCL as a function of knee flexion. The displacement revealed the different strain patterns of the anterior and posterior borders of the MCL [5, 6, 7, 8].

DVRTs and Hall-Effect sensors are relatively bulky and heavy and of low sensitivity. Recently, a fibre-optic sensor, which measures displacement using optic technology, was used in cadaver knees to measure ligament deformation in a variety of simulated postures. The fibre optic cable was compressed when the ligament stretched, which modulated the light intensity through the fibre [9].

To totally remove the invasiveness of sensor insertion, computer vision was also used for detecting ligament deformation in cadaveric knees. Ref [10] reported using magnetic resonance imaging (MRI) and video-based experimental measurements to study knee ligaments subject to six loading scenarios. The ligament behaviour was identified as transversely isotropic hyperelastic.

A number of implantable transducers have been used in vivo to investigate the strains of the knee ligament under different loads. These devices are generally wrapped around, or sewn onto the ligament. For example, a DVRT was sewn onto the side of the knee ligament and measured the displacement of the portion of the ligament when it stretched. The ligament strain was inferred from the ligament's displacement [11, 12, 13]

A Hall-Effect transducer was applied to the ACL of 13 subjects to test the efficacy of 7 functional knee braces, which are widely used to protect injured or reconstructed ACL. Two braces were found to provide some strain-shielding protection under low loads, and none of the braces produced adverse effect on the ACL [14].

A piezoelectric transducer, which measures changes in pressure, was used to evaluate an isometry measurement in an ACL substitute on 10 subjects under anaesthesia when the knees were passively moved through the range of 0 to 100 $^{\circ}$ [15]

A conductive rubber sensor, which uses pressure-sensitive conductive rubber that alters its resistance due to elongation or by external force, was used to provide quantitative strain measurements on the ligaments to surgeons during total knee arthroplasty, which traditionally relied on the subjective feedback for correct ligament balancing [16, 17].

An ultrasonic sensor was used to quantitatively evaluate the ACL in situ by introducing an ultrasonic probe into the knee joint under arthroscopy and analyzing the A-mode echogram by means of wavelet transformation [18]. Ultrasonic sensors were also used to compare the elasticity of normal human ACLs with a variety of ACL graft substitutes [19].

However, identifying the properties of ligaments experimentally requires implanting a physical sensor, which is not only expensive and time-consuming but also could lead to fibrous healing reactions. These sensors suffer from issues such as difficulty in calibration and sensitivity to the geometry of the insertion site. They have several additional limitations, including being bulky and shortening the ligament slightly when it kinks around the buckle. Further, the sensor's dimension and position can only reflect the local properties of the ligament instead of a whole [20].

In recent years, musculoskeletal simulation has increased to become an important tool because simulation can include more variables and predict the changes in knee dynamics after ligament craft or when the knee is subject to external device such as a brace or an exoskeleton.

In the early days of development, the knee joint was normally modelled in two dimensions (2D), where the profiles of the joint surfaces represented by polynomials and the joint ligaments were treated as nonlinear springs. It was shown that simulation results on ligament stretches under different loads were comparable to experiment results [21].

With the increase of computing power, the knee joint was then modelled in three dimensions (3D), where finite element method (FEM) was used to simulate the stress of the ligament behaviour under passive/active movements. The 3D geometrical models of the bones were usually built from 3D CT scans and the parameters of the ligaments were obtained from experimental results [22, 23, 24, 25, 26, 27].

Despite the advances in the modelling and simulation of the knee ligaments, these computational models need to be verified using instrumented analogue knees [23]. Recently rehabilitation/assistive robotic leg exoskeletons, as well as functional knee braces, are becoming increasingly popular as the percentage of people sustaining injury to the knee increases and people desire for powered leg exoskeletons to carry heavier loads or run faster/longer. But these devices have the potential to cause damage to the knee, so it is essential to understand the strain of the

knee ligaments effected by these devices [28].

Recent advancements in 3D scanning and printing technologies take this process to a new level by allowing subject-specific models to be created, leading to an anatomically correct knee joint capable of measuring the interaction between the osseous joint structure and the surrounding passive ligaments. Rapid prototyping knee models reduce the level of uncertainty from 3D computational models [29, 30, 31, 32].

An instrumented analogue model of a knee joint from 3D rapid prototyping has a wide range of applications, for example, aiding in validating a robotic leg exoskeleton before in-vivo testing to reduce the risks and cost of such testings. It can also serve as a training aid for health workers to better understand the knee dynamics and aid in diagnosis, treatment, and rehabilitation of joint injuries such as torn ligaments.

In this work, we presented an analog knee joint that provides real-time displacement measurements of the four main ligaments: ACL, PCL, MCL, and LCL. This paper is organized as follows. Section 1 reviewed how the knee ligament strains were measured. Section 2 describes design considerations, and Section 3 describes 3D modeling of the knee. Section 4 presents spring and cord selection, rotary encoder mechanism, knee angle sensor linkage, and mechanical assembly. Section 5 presents results and discussion. Section 6 concludes this paper.

2 MATERIALS AND METHODS

2.1 Design Considerations

We aimed to design and develop an instrumented analogue knee model via 3D rapid prototyping that quantifies the strains of the four main knee ligaments in real-time when the knee moves from full extension to full flexion.

The femur and tibia-fibula bones were printed using acrylonitrile butadiene styrene (ABS) for its strength and rigidity, and the mensici was printed with using thermoplastic polyurethane (TPU) for its elasticity. We decided not to use metal 3D printing because this would increase the cost of the prototyping remarkably.

The ligaments are fastened between the femur and the tibia/fibula and have an elastic, spring-

like constitution that keeps them tight at most knee angles. Ligament stiffness is slightly non-linear. Initially, as force is applied to a slack ligament, it has a low stiffness in the toe region before entering a linear elastic region. As the force increases, the ligament stiffness lowers as it enters the plastic region, during which the ligament fibres start breaking, and then finally it reaches its catastrophic failure point [2, 33].

While the LCL has only one main fiber bundle, each of the ACL, PCL, and MCL consists of two major fiber bundles. The ACL consists of the anteromedial bundle (aACL) and posterolateral bundle (pACL). When the knee is extended, the pACL is tight and the aACL is moderately lax. As the knee is flexed, the aACL tightens and the pACL relaxes [34]. The PCL consists of the anterolateral bundle (aPCL) and posteromedial bundle (pPCL). The aPCL and pPCL act primarily during knee flexion and extension, respectively. The aPCL is six times as strong as the pPCL [35]. The MCL consists of the superficial bundle (sMCL) and deep bundle (dMCL). The anterior and posterior of the sMCL and dMCL have a reciprocal function during the stance phase of gait [36].

We chose to use a non-stretchable cord to serve as one of the seven major fiber bundles, to the ends of which a spring is affixed to provide the desired stiffness of the structure. An additional advantage is that the flexible cord is able to thread through the curved section in the bones.

We decided to quantify the displacement of each of the seven cords via a rotary encoder with a pulley system, where the cord is wrapped around the encoder output shaft. When the cord is tightened, it stretches the spring and rotates the encoder shaft so that linear motion of the cord is converted into rotational motion of the encoder shaft.

2.2 Ligament Trajectories

We obtained the 3D scans of the femur, tibia, fibula, and menisci of a right leg and subsequently modified these scans to allow for sensors, springs, and bolts. The modified 3D models of these parts can be seen in the Appendix.

Fig. 2 shows the ligament trajectories, where the menisci has been removed to reveal the entry and exit holes. Each of the circular holes is of a diameter of $6mm$ with its center following a gentle curve, allowing Polytetrafluoroethylene (PTFE) tubing inserted through the hole to serve as cord guide, which protects the hole surface and reduces friction.

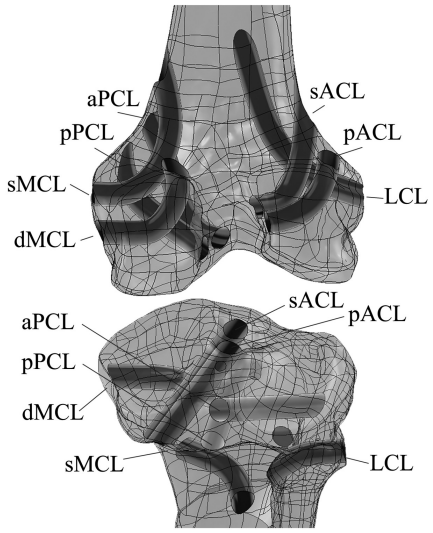

Fig. 2. The ligament trajectories

Fig. 3 shows the ligament-system assembly, where each of the seven ligament cords has its one end attached to one spring located inside the thigh shell, wraps around one encoder shaft, passes through a PTFE tube in a hole in the femur and a PTFE tube in a hole in the tibia-fibula, and then has its another end anchored onto a threaded rod located inside the shin shell, which is used to set the cord's pretension. A microcontroller processes and stores the real-time displacements of the seven cords.

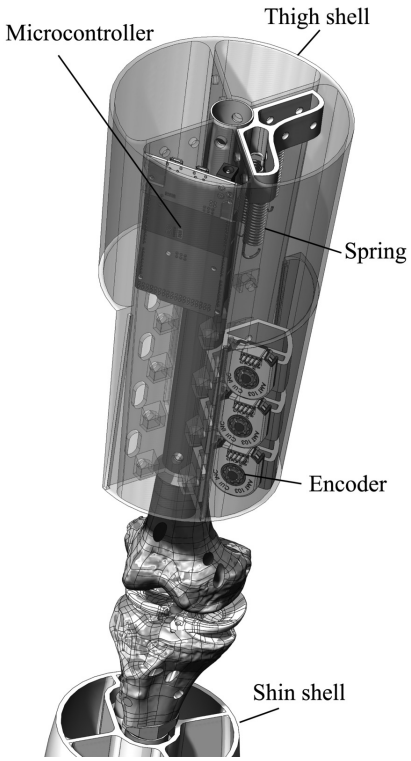

Fig. 3. The encoder-based measurement system of ligament displacements

2.3 Springs

The stiffness of the seven main ligament fiber bundles vary from $60\ N/mm$ (the MCL and LCL) to $350\ N/mm$ (aPCL and aACL) [37]. The stiffnesses of the seven springs corresponding to the seven main ligament fiber bundles were chosen to be reduced by a factor of 10 as using the actual stiffnesses to tension the cords would impose rather high pressure on the bones, which were 3D printed using ABS, causing them to deform permanently or even crack. The actual knee ligament stiffnesses and the spring stiffnessess are shown in Table 1.

Fibre bundles	Desired stiffnesses	Spring stiffnesses
aACL	350.0	35.6
pACL	200.0	20.3
aPCL	350.0	35.5
pPCL	80.0	8.06
dMCL	60.0	6.1
sMCL	60.0	6.1
LCL	60.0	6.1

Table 1. Spring stiffnesses (N/mm) chosen proportionally to the fibre-bundle stiffnesses (N/mm)

2.4 Ligament Cords

Each ligament cord consists of three strands of mono-filament fishing line of diameter $1.0\ mm$ with a stretch rate of $455.0\ N/mm$. When the knee moves from full extension to full flexion, the ligament subject to the largest force is the aACL, which is elongated by about $1.0\ mm$, exerting a force of $35.6\ N$ on the cord given the spring stiffness is $35.6\ N/mm$ (Table 1). This force is only 2.6% of the combined fishing line rating, so the stretch of each ligament cord is negligible.

2.5 Rotary Encoders

One high-resolution incremental rotary encoder is used to measure the displacement of one ligament cord, which wraps around the flywheel of the encoder via a pulley system. The ligament cord is pretensioned using an spring with a desired stiffness. When the ligament cord is subject to the force exerted by the knee movement, it stretches the spring and subsequently rotates the encoder shaft. This mechanism converts the linear motion of the cord into the rotational motion of the rotary encoder shaft, as in Fig. 4.

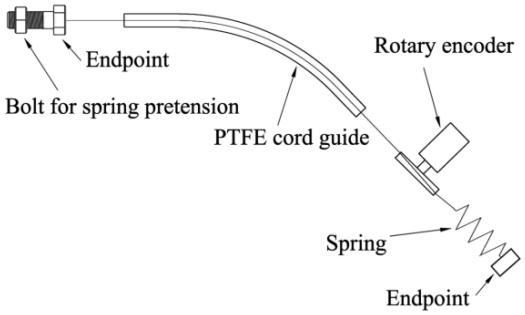

Fig. 4. The rotary encoder mechanism

2.6 Knee Angle Sensor

The knee flexion angles need to be measured to quantify the ligament lengths. We designed an open-loop two-bar linkage consisting of three revolute (R) joints, where a rotary encoder is mounted on the middle revolute joint. One end of the linkage can be clipped on the thigh shell and the other end on the shin shell, so that it can be removed or mounted conveniently.

When the two-bar linkage is mounted on the leg, the thigh, the shin, and the two bars of the linkage form a closed-loop four-bar linkage with the knee serves as one of the four joints. Further, the lengths of the bars were designed in such a way that AB and AD are equal, so are BC and DC. Hence, the four-bar linkage is of a a diamond shape, leading to the changes in the knee flexion/extension joint angle θ_1 are equal to those in its opposite joint angles θ_2 that are measured by the rotary encoder., as in Fig. 5.

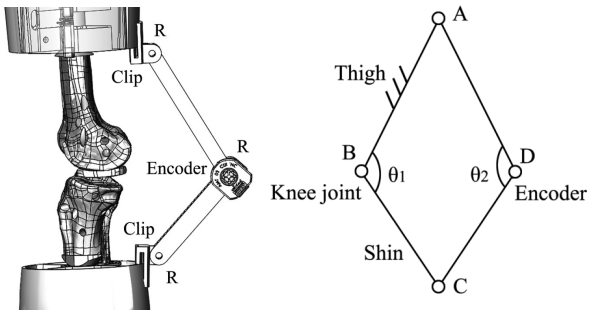

(a) (b)

Fig. 5. The knee angle sensor (a) The sensor linkage clipped on the leg (b) The closed-loop fourbar linkage of a diamond shape

2.7 Mechanical Assembly

Fig. 6 shows a prototype of the leg model with a close-up of the knee joint. The ligament cords can be seen inside the PTFE tubing, passing between the two bones and exiting down toward the tensioners. One piece of the shell is moved to reveal the internal support structure. The encoder and spring mounts are shown in position on those rods.

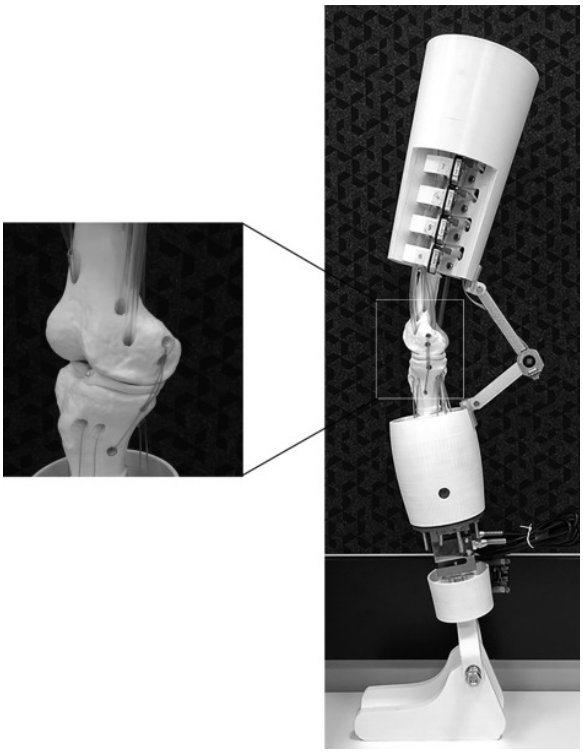

Fig. 6. The prototype of the leg model with a close-up view of the knee joint

3 RESULTS

We pretensioned the springs connected to the ligament cords make them taut at their slackest points, and used an Arduino Due© to obtain the readings from the eight encoders (seven for the ligament cords and one for the knee angles), which were converted to the displacements of the ligament cords simultaneously when the knee moved from full extension to full flexion. The displacements of the 7 fiber bundles against the knee flexion angles are shown in Fig. 7.

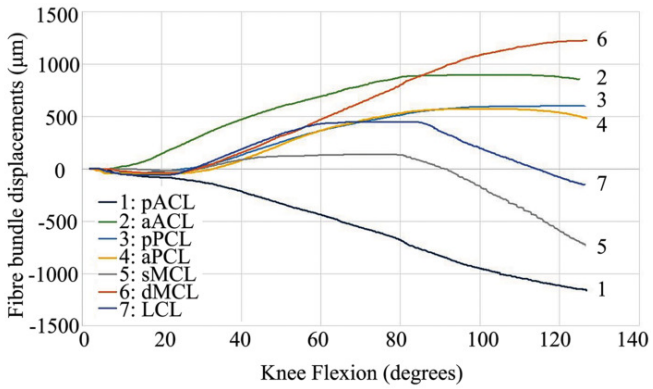

Fig. 7. The displacements of the 7 fibre bundles against the knee flexion angles

3.1 The ACL: the aACL and pACL Cords

Fig. 8 shows the displacements of the cords serving as the aACL and pACL fiber bundles, respectively, against knee flexion angles.

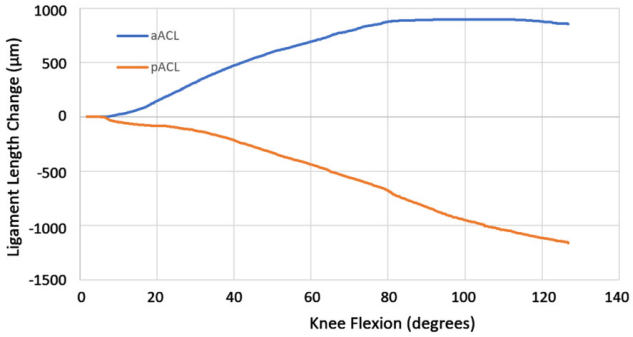

Fig. 8. The displacements of the ACL ligament cords when the knee moves from full extension to full flexion

The aACL cord stretches and the pACL cord slackens during knee flexion: the trends of the two displacement curves agree with those reported in [38], where the displacements of the aACL and pACL were measured *in vivo* after an operation with arthroscopically placed sterile Hall-effect strain transducers.

The Figure 44 in [12] showed an ACL strain graph for the two fiber bundles combined into a single unit, where the displacements were required *in vivo* with a DVRT attached to the anteromedial aspect of the ACL. The slackening as the flexion angle increases implies that the pACL is the

dominant fiber bundle: less stiff and thus stretches more under the same load. Fig. 8 shows the same characteristic: the absolute value of the maximum displacement of the pACL is about -1100 μm and that of the aACL is about 900 μm in full flexion.

3.2 The PCL: the aPCL and pPCL Cords

Fig. 9 shows the displacements of the cords serving as the aPCL and pPCL fiber bundles, respectively, against knee flexion angles.

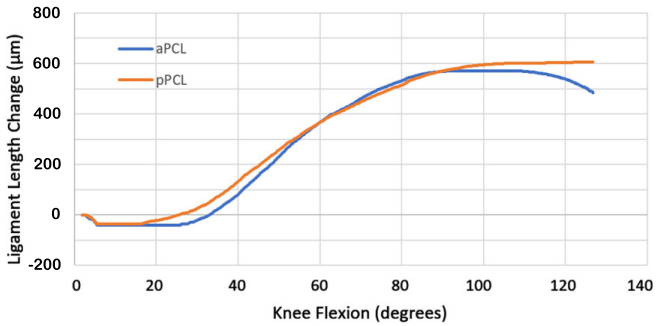

Fig. 9. The displacements of the PCL ligament cords when the knee moves from full extension to full flexion

The displacement curves of the aPCL and pPCL cords are similar, slackening by 50 μm over the first 30°, steadily tightening to a maximum of 500 μm at 90°, where the pPCL cord plateaus while the aPCL cord stretches back by about 100 μm at full flexion.

The stress-strain of the aPCL and pPCL fiber bundles in the Figure 2 of [39], where the displacements were generated by a validated nonlinear 3D tibiofemoral model of the knee joint, showed similar profiles to to those in Fig. 9: they initially slowly rise steadily rises from 0 to 20% at about $90°$ and then drops to 15%. This implies that the length of the aPCL fiber bundle increases steadily until $90°$ and keeps increasing at a lower rate until full flexion.

3.3 The MCL: the dMCL and sMCL Cords

Fig. 10 shows the displacements of the cords serving as the dMCL and sMCL fiber bundles, respectively, against knee joint angles.

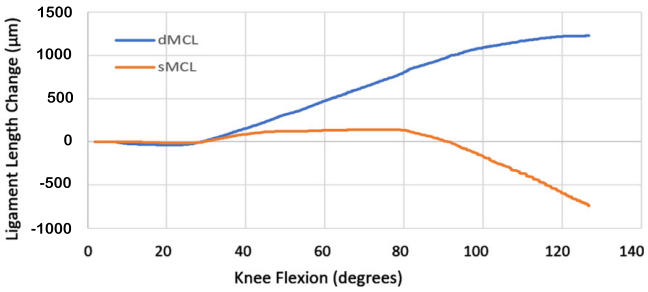

Fig. 10. The extension of the MCL ligament when the knee moves from full extension to full flexion

The two displacement curves start off nearly flatly, and at round 30° the dMCL cord tightens continuously, reaching $1200\mu m$ while the the sMCL cord bears zero force until 80° and then slackens almost linearly to $-700\ \mu m$.

The two curves in Fig. 10 show the same trend in [36], which used a dual fluoroscopic imaging system (DFIS) to determine knee kinematics during the stance phase of gait and reported that the sMCL and dMCL had a reciprocal function during knee flexion, implying that one slackened while the other one tightened.

The sMCL curve in Fig. 10, which only starts to decrease at about 80° until full flexion, partially agrees with the strain behavior reported in [40], which used a 3D fluoroscope to captur images of the knee *in-vivo* to calculate the relative fibre bundle elongations. The strain reached maximum at full extension and decreased nearly linearly to about 140°.

Further, the sMCL curve shows a similar profile to that reported in [41], which used a 3D dynamic model of the knee to calculate the elongtations of the ligaments. It reported the curve started off with a nearly flat curve and dropped off at around 80°.

The dMCL in [42], which used MR images to construct a 3D model of each knee with 3D modeling software and then generates the displacements of the fibre bundles, was split into anterior, middle and posterior sections. The anterior section has a steadily increasing length, just like the dMCL curve in Fig. 10, but it is hard to quantify how the three sections interact when combined into a single dMCL fiber bundle.

3.4 The LCL Cord

Fig. 11 shows the displacements of the cord serving as the LCL against knee joint angles. The displacement curve remains flat in the first $30°$, climbs up and reaches a plateau at $60°$, and then decreases nearly linearly until full knee flexion.

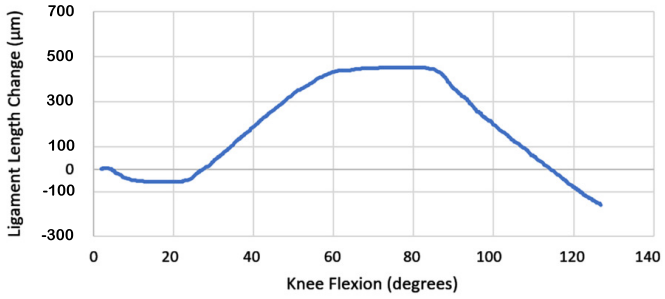

Fig. 11. The extension of the LCL ligament when the knee moves from full extension to full flexion

The Ref [42] reported that the length of the LCL increased by 7% at $90°$ of flexion from full extension and decreased by 8% from the peak at full flexion. The reported profile agrees with that in Fig. 11.

4 DISCUSSION

The reported knee-joint model is not subject-specific. We used plastic casted replicas of a male adult donor, from which 3D models were generated via 3D scanning, and these models were subsequently modified in Solidworks™. However, subject-specific models can be generated straightforwardly from computed tomography (CT) scans, and similar modifications can be applied to these models.

The attachment locations of the 7 fibre bundles were sourced from literature. The attachment locations of the aACL and pACL were from [43], those of aPCL and pPCL from [44], those of aMCL and dMCL from [45], and those of LCL from [46].

It was time-consuming to 3D print the bones. we used an Ultimaker^2 Extended+™ consumer 3D printer and set the nozzle size at $0.4\,mm$, print quality at $0.1\,mm$, and infill density at 50%, and the material was Acrylonitrile butadiene styrene (ABS) filament. It took about 21 hours and 18

hours to print out the femur and tibia-fibula, respectively, though the material cost was negligent.

We chose not to install the patella as its primary purpose is to increase the leverage that the quadriceps tendon can exert on the femur, which is beyond the scope of this work. We also believed that a customized silicone sleeve would be required to cover the whole knee joint to keep the patella at the right position. This sleeve would in turn increase the total cost of the knee model significantly.

We used the AMT103-V™ capacitive rotary incremental encoders, which have a resolution of 2048 pulse per revolution (PPR), and because they are quadrature encoders, giving an effective resolution of 8192 signals per revolution. These encoders can accept various shaft diameters, and the diameter selected for this project was $6\ mm$, giving a resolution of $2.3\ \mu m$.

We manually activated the knee joint from full extension to full flexion in about 4 seconds. The geometries of the articular surfaces of the tibia, femur and the pre-tensioned cords helped to facilitate the knee internal-external rotation.

We only measured the cord displacements when the knee rotated from full extension to full flexion, where the results were corroborated by published data, the majority of which focused on this range of motion. Because the sensors (encoders) we chose and mechanical design (using springs), the process displayed repeatability of results. Hysteresis, a common issue related to sensing, did not occur.

The main advantages of this work is the knee model is able to simultaneously measure the displacments of the 7 fibre bundles against knee flexion—this has only been achived by computational models in the past. Another advantage is it is easy to replace a spring with one with different stiffness, for example, to simulate ligament injury. This could be used to examine the effects of this injured ligament on other ligaments.

Some limitations should be noted. First, we did not investigate the the sensitivities of the results to a variation in the entry and exit holes. We designed the entry and exit holes such that the cords could be threaded through, would not tangle during knee flexion/extension, and the passages were all gently curved to reduce friction. Second, we used three thin cords together to serve as a fibre bundle, where friction among them was unavoidable. Thicker and non-extensible materials should

be sourced. Third, the knee angle sensor provided only approximate angle readings, as the knee joint is not a simple 2D pin joint. A more sophisticated mechanism should be investigated.

5 CONCLUSION

We designed and prototyped a knee model that is able to measure the displacements of the 7 major fibre bundles—the aACL, pACL, aPCL, pPCL, dMCL, sMCL, and LCL—against knee flexion. The proposed approach in modeling and rapid prototyping could be used to develop subject-specific knee models by printing out the femur, tibia, and menisci from 3D medical imaging scans of a subject and choosing the springs with desired stiffnesses for the fiber bundles. The knee model is able to quantify the displacement experienced by the fiber bundles simultaneously and could find applications in health workforce education and training and work place injury detection.

ACKNOWLEDGEMENTS

Mr. Alex Charles Kovacs's work on design and modeling is greatly acknowledged. The support by the Australian Research Council Grant DE170101062 and National Natural Science Foundation of China under (Grant 51975451) is greatly acknowledged.

REFERENCES

[1] Morrison, J. B., 1970. "The mechanics of the knee joint in relation to normal walking". *Journal of Biomechanics,* **3**(1), pp. 51–61.

[2] Robinson, J. R., Bull, A. M. J., and Amis, A. A., 2005. "Structural properties of the medial collateral ligament complex of the human knee". *Journal of Biomechanics,* **38**(5), pp. 1067–1074.

[3] Butler, D. L., Grood, E. S., Noyes, F. R., Zernicke, R. F., and Brackett, K., 1984. "Effects of structure and strain measurement technique on the material properties of young human tendons and fascia". *Journal of Biomechanics,* **17**(8), pp. 579–596.

[4] Withrow, T. J., Huston, L. J., Wojtys, E. M., and Ashton-Miller, J. A., 2006. "The relationship

between quadriceps muscle force, knee flexion, and anterior cruciate ligament strain in an in vitro simulated jump landing". *The American Journal of Sports Medicine,* **34**(2), pp. 269–274.

[5] Arms, S., Boyle, J., Johnson, R., and Pope, M., 1983. "Strain measurement in the medial collateral ligament of the human knee: An autopsy study". *Journal of Biomechanics,* **16**(7), pp. 491–496.

[6] Singerman, R., Dean, J. C., Pagan, H. D., and Goldberg, V. M., 1996. "Decreased posterior tibial slope increases strain in the posterior cruciate ligament following total knee arthroplasty". *The Journal of Arthroplasty,* **11**(1), pp. 99–103.

[7] Arms, S. W., Pope, M. H., Johnson, R. J., Fischer, R. A., Arvidsson, I., and Eriksson, E., 1984. "The biomechanics of anterior cruciate ligament rehabilitation and reconstruction". *The American Journal of Sports Medicine,* **12**(1), pp. 8–18.

[8] Fleming, B., Beynnon, B., Howe, J., McLeod, W., and Pope, M., 1992. "Effect of tension and placement of a prosthetic anterior cruciate ligament on the anteroposterior laxity of the knee". *Journal of Orthopaedic Research,* **10**(2), pp. 177–186.

[9] Ren, L., Song, G., Conditt, M., Noble, P. C., and Li, H., 2007. "Fiber bragg grating displacement sensor for movement measurement of tendons and ligaments". *Applied Optics,* **46**(28), pp. 6867–6871.

[10] Phatak, N. S., Sun, Q., Kim, S.-E., Parker, D. L., Kent Sanders, R., Veress, A. I., Ellis, B. J., and Weiss, J. A., 2007. "Noninvasive determination of ligament strain with deformable image registration". *Annals of Biomedical Engineering,* **35**(7), pp. 1175–1187.

[11] Fleming, B. C., Renstrom, P. A., Beynnon, B. D., Engstrom, B., Peura, G. D., Badger, G. J., and Johnson, R. J., 2001. "The effect of weightbearing and external loading on anterior cruciate ligament strain". *Journal of Biomechanics,* **34**(2), pp. 163–170.

[12] Fleming, B. C., Beynnon, B. D., Renstrom, P. A., Peura, G. D., Nichols, C. E., and Johnson, R. J., 1998. "The strain behavior of the anterior cruciate ligament during bicycling". *The American Journal of Sports Medicine,* **26**(1), pp. 109–118.

[13] Heijne, A., Fleming, B., Renstrom, P., Peura, G., Beynnon, B., and Werner, S., 2004. "Strain on the anterior cruciate ligament during closed kinetic chain exercises.". *Medicine and Sci-*

ence in Sports and Exercise, **36**(9), pp. 935–941.

[14] Beynnon, B. D., Pope, M. H., Wertheimer, C. M., Johnson, R. J., Fleming, B. C., Nichols, C. E., and Howe, J. G., 1992. "The effect of functional knee-braces on strain on the anterior cruciate ligament in vivo". *The Journal of bone and joint surgery. American volume,* **74**(9), pp. 1298–1312.

[15] Good, L., and Gillquist, J., 1993. "The value of intraoperative isometry measurements in anterior cruciate ligament reconstruction: An in vivo correlation between substitute tension and length change". *Arthroscopy: The Journal of Arthroscopic and Related Surgery,* **9**(5), pp. 525–532.

[16] Som, M. H. M., Nagamune, K., Kamiya, T., Kawaguchi, S., Takayama, K., Matsumoto, T., Kuroda, R., and Kurosaka, M., 2014. "A development of force distribution measurement system with high resolution for total knee arthroplasty". *Journal of Advanced Computational Intelligence and Intelligent Informatics,* **18**(2), pp. 213–220.

[17] Nusser, M., Fehle, A., and Senner, V., 2012. "Preliminary studies for validation of a novel sensor fiber to measure forces in artificial knee ligaments". *Procedia Engineering,* **34**, pp. 236–241.

[18] Hattori, K., Mori, K., Habata, T., Takakura, Y., and Ikeuchi, K., 2003. "Measurement of the mechanical condition of articular cartilage with an ultrasonic probe: quantitative evaluation using wavelet transformation". *Clinical Biomechanics,* **18**(6), pp. 553–557.

[19] Krishna, K. V., and Vidyasagar, J. V. S. "Biomechanical analysis of anterior cruciate ligament graft substitutes". In Proceedings of the First Regional Conference, IEEE Engineering in Medicine and Biology Society and 14th Conference of the Biomedical Engineering Society of India. An International Meet, pp. SPC3–SPC4.

[20] Ravary, B., Pourcelot, P., Bortolussi, C., Konieczka, S., and Crevier-Denoix, N., 2004. "Strain and force transducers used in human and veterinary tendon and ligament biomechanical studies". *Clinical Biomechanics,* **19**(5), pp. 433–447.

[21] Moeinzadeh, M. H., Engin, A. E., and Akkas, N., 1983. "Two-dimensional dynamic modelling of human knee joint". *Journal of Biomechanics,* **16**(4), pp. 253–264.

[22] Limbert, G., Taylor, M., and Middleton, J., 2004. "Three-dimensional finite element modelling of the human acl: simulation of passive knee flexion with a stressed and stress-free acl". *Journal of Biomechanics,* **37**(11), pp. 1723–1731.

[23] Guess, T. M., and Maletsky, L. P., 2005. "Computational modelling of a total knee prosthetic loaded in a dynamic knee simulator". *Medical Engineering and Physics,* **27**(5), pp. 357–367.

[24] Xu, H., Bloswick, D., and Merryweather, A., 2015. "An improved opensim gait model with multiple degrees of freedom knee joint and knee ligaments". *Computer Methods in Biomechanics and Biomedical Engineering,* **18**(11), pp. 1217–1224.

[25] Sikidar, A., and Kalyanasundaram, D., 2019. "An open-source plugin for opensim® to model the non-linear behaviour of dense connective tissues of the human knee at variable strain rates". *Computers in Biology and Medicine,* **110**, pp. 186–195.

[26] Akalan, N. E., Özkan, M., and Temelli, Y., 2008. "Three-dimensional knee model: Constrained by isometric ligament bundles and experimentally obtained tibio-femoral contacts". *Journal of Biomechanics,* **41**(4), pp. 890–896.

[27] Kang, K. T., Koh, Y. G., Jung, M., Nam, J. H., Son, J., Lee, Y. H., Kim, S. J., and Kim, S. H., 2017. "The effects of posterior cruciate ligament deficiency on posterolateral corner structures under gait- and squat-loading conditions: A computational knee model". *Bone and joint research,* **6**(1), pp. 31–42.

[28] Shen, Z., Sam, S., Allison, G., and Cui, L., 2018. "A simulation-based study on a clutch-spring mechanism reducing human walking metabolic cost". *International Journal of Mechanical Engineering and Robotics Research,* **7**(1), pp. 55–60.

[29] He, J., Li, D., Lu, B., Wang, Z., and Zhang, T., 2006. "Custom fabrication of a composite hemi-knee joint based on rapid prototyping". *Rapid Prototyping Journal,* **12**(4), pp. 198–205.

[30] Szojka, A., Lalh, K., Andrews, S. H. J., Jomha, N. M., Osswald, M., and Adesida, A. B., 2017. "Biomimetic 3d printed scaffolds for meniscus tissue engineering". *Bioprinting,* **8**, pp. 1–7.

[31] Beckmann, J., Steinert, A., Zilkens, C., Zeh, A., Schnurr, C., Schmitt-Sody, M., and Gebauer, M., 2016. "[partial replacement of the knee joint with patient-specific instruments and implants (conformis iuni, iduo)]". *Der Orthopade,* **45**(4), pp. 322–330.

[32] Park, J. H., Lee, Y., Shon, O.-J., Shon, H. C., and Kim, J. W., 2016. "Surgical tips of intramedullary nailing in severely bowed femurs in atypical femur fractures: Simulation with 3d printed model". *Injury,* **47**(6), pp. 1318–1324.

[33] Woo, S. L. Y., Abramowitch, S. D., Kilger, R., and Liang, R., 2006. "Biomechanics of knee ligaments: injury, healing, and repair". *Journal of Biomechanics,* **39**(1), pp. 1–20.

[34] Petersen, W., and Zantop, T., 2007. "Anatomy of the anterior cruciate ligament with regard to its two bundles". *Clinical orthopaedics and related research,* **454**, pp. 35–47.

[35] Race, A., and Amis, A. A., 1994. "The mechanical properties of the two bundles of the human posterior cruciate ligament". *Journal of Biomechanics,* **27**(1), pp. 13–24.

[36] Liu, F., Gadikota, H. R., Kozánek, M., Hosseini, A., Yue, B., Gill, T. J., Rubash, H. E., and Li, G., 2011. "In vivo length patterns of the medial collateral ligament during the stance phase of gait". *Knee surgery, sports traumatology, arthroscopy : official journal of the ESSKA,* **19**(5), pp. 719–727.

[37] Mommersteeg, T. J. A., Blankevoort, L., Huiskes, R., Kooloos, J. G. M., and Kauer, J. M. G., 1996. "Characterization of the mechanical behavior of human knee ligaments: A numerical-experimental approach". *Journal of Biomechanics,* **29**(2), pp. 151–160.

[38] FU, F. H., HARNER, C. D., JOHNSON, D. L., MILLER, M. D., and WOO, S. L.-Y., 1993. "Biomechanics of knee ligaments: Basic concepts and clinical application". *JBJS,* **75**(11), pp. 1716–1727.

[39] Mesfar, W., and Shirazi-Adl, A., 2005. "Biomechanics of the knee joint in flexion under various quadriceps forces". *The Knee,* **12**(6), pp. 424–434.

[40] Edwards, R. G., Lafferty, J. F., and Lange, K. O., 1970. "Ligament strain in the human knee joint". *Journal of Basic Engineering,* **92**(1), pp. 131–136.

[41] Kim, S., 1998. "Three-dimensional dynamic model of the knee". *KSME International Journal,* **12**(6), p. 1041.

[42] Park, S. E., DeFrate, L. E., Suggs, J. F., Gill, T. J., Rubash, H. E., and Li, G., 2005. "The change in length of the medial and lateral collateral ligaments during in vivo knee flexion". *The Knee,* **12**(5), pp. 377–382.

[43] Lee, Y. S., Lee, S.-W., Nam, S. W., Oh, W. S., Sim, J. A., Kwak, J. H., and Lee, B. K., 2012. "Analysis of tunnel widening after double-bundle acl reconstruction". *Knee Surgery, Sports Traumatology, Arthroscopy,* **20**(11), pp. 2243–2250.

[44] Harner, C. D., Xerogeanes, J. W., Livesay, G. A., Carlin, G. J., Smith, B. A., Kusayama, T., Kashiwaguchi, S., and Woo, S. L., 1995. "The human posterior cruciate ligament complex: an interdisciplinary study. ligament morphology and biomechanical evaluation". *Am J Sports Med,* **23**(6), pp. 736–45.

[45] LaPrade, R. F., Engebretsen, A. H., Ly, T. V., Johansen, S., Wentorf, F. A., and Engebretsen, L., 2007. "The anatomy of the medial part of the knee". *JBJS,* **89**(9).

[46] LaPrade, R. F., Ly, T. V., Wentorf, F. A., and Engebretsen, L., 2003. "The posterolateral attachments of the knee: a qualitative and quantitative morphologic analysis of the fibular collateral ligament, popliteus tendon, popliteofibular ligament, and lateral gastrocnemius tendon". *Am J Sports Med,* **31**(6), pp. 854–60.

A APPENDIX: 3D MODELING OF THE KNEE

A.1 Femur Construction

The anterior, posterior, lateral, and medial views of the femur are shown in Fig. A.1. The entry and exit holes can be seen to allow ligament cords to thread through the bone and go straight up for their ends to be attached to the springs at the top end. The exit holes are located in such a way to prevent the cords from entangling while the knee is in motion.

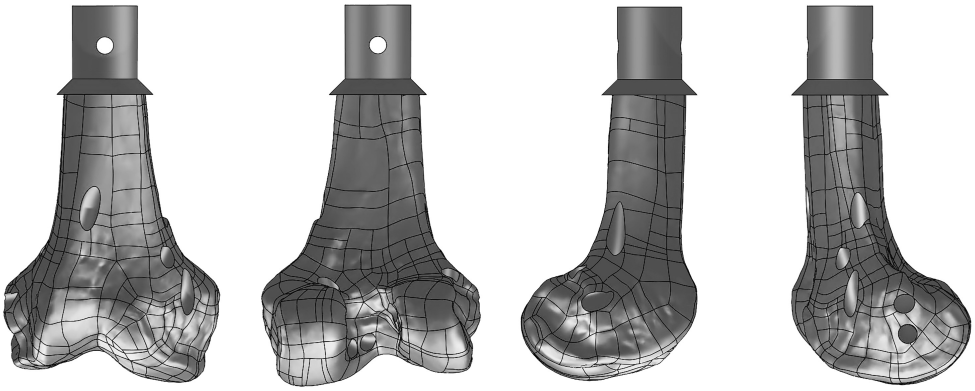

(a) (b) (c) (d)

Fig. A.1. The 3D model of the femur with holes for ligament cords to thread through: (a) Anterior view (b) Posterior view (c) Lateral view (d) Medial view

A.2 Tibia and Fibula Construction

The anterior, posterior, lateral, and medial views of the tibia-fibula are shown in Fig. A.2. The entry and exit holes allow ligament cords to thread through the bone and go down for their ends to be attached to the bottom of the leg.

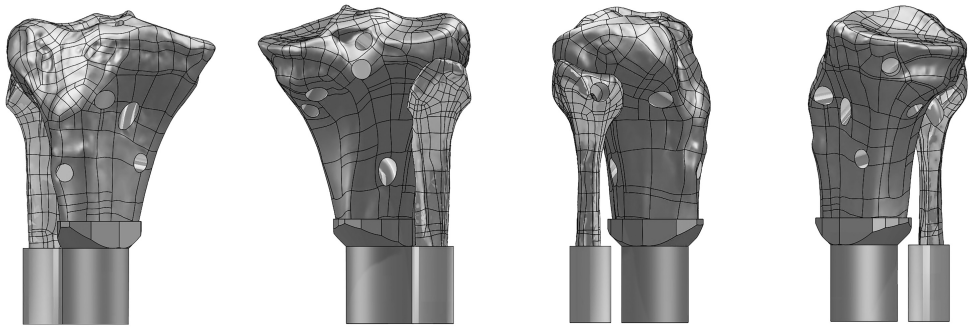

(a) (b) (c) (d)

Fig. A.2. The 3D model of the tibia-fibula with holes for ligament cords to thread through: (a) Anterior view (b) Posterior view (c) Lateral view (d) Medial view

A.3 Menisci

Three mounting holes of diameter $3\,mm$ were added to the menisci to mount it on the medial condyle of the tibia, as in Fig. A.3.

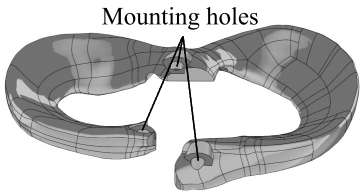

Fig. A.3. The menisci with three mounting holes

LIST OF FIGURES

LIST OF TABLES